

**Supporting information**

**High-Rate Lithium-Sulfur Battery Assisted with Ultrafine La<sub>2</sub>O<sub>3</sub>  
Nanoparticles Decorated and Nitrogen-Enriched Mesoporous Carbons**

*Fugen Sun<sup>a</sup>, Jitong Wang<sup>a</sup>, Donghui Long<sup>a\*</sup>, Wenming Qiao<sup>a</sup>, Licheng Ling<sup>a</sup>, Chunxiang<sup>b</sup>  
Lv and Rong Cai<sup>b\*</sup>*

*<sup>a</sup>State Key Laboratory of Chemical Engineering, East China University of Science and Technology,  
Shanghai 200237*

*<sup>b</sup>National Engineering Laboratory for Carbon Fiber Preparation Technology, Institute of Coal Chemistry,  
Chinese Academy of Sciences,  
Taiyuan 030001*

\*To whom correspondence should be addressed. E-mail: [longdh@mail.ecust.edu.cn](mailto:longdh@mail.ecust.edu.cn); [cair@sxicc.ac.cn](mailto:cair@sxicc.ac.cn)

## **Content:**

**Table S1.** Chemical nature of the NMCs and MCs.

**Table S2.** Pore structure parameters of the MC/La<sub>2</sub>O<sub>3</sub> composites and NMC/La<sub>2</sub>O<sub>3</sub> composites.

**Figure S1.** XPS survey spectra of NMCs and MCs and high-resolution XPS N<sub>1s</sub> spectra of NMCs.

**Figure S2.** TEM image of 10La-MC composites.

**Figure S3.** Coulombic efficiency of NMC/La<sub>2</sub>O<sub>3</sub>/S composites at 0.2 C, 1 C, 3 C and 5 C.

**Figure S4.** EIS before 1st cycle of NMC/La<sub>2</sub>O<sub>3</sub>/S composites.

**Figure S5.** Thermogravimetric analysis (TGA) curves of MC/La<sub>2</sub>O<sub>3</sub>/S composites.

**Figure S6.** Typical cyclic voltammogram of nitrogen-free MC/La<sub>2</sub>O<sub>3</sub>/S composites at 0.2 mV s<sup>-1</sup> and 2 mV s<sup>-1</sup>.

**Figure S7.** Initial charge-discharge curves of nitrogen-free MC/La<sub>2</sub>O<sub>3</sub>/S composites at 0.2 C, 1 C, 3 C and 5 C.

**Figure S8.** Cycle stability of nitrogen-free MC/La<sub>2</sub>O<sub>3</sub>/S composites at 0.2 C, 1 C, 3 C and 5 C.

**Figure S9.** EIS before 1st cycle of nitrogen-free MC/La<sub>2</sub>O<sub>3</sub>/S composites.

**Table S1.** Chemical nature of the NMCs and MCs

Samples	Element analysis				XPS			$S_{\text{BET}}^{[d]}$ $\text{m}^2 \text{g}^{-1}$	$V_{\text{T}}^{[e]}$ $\text{cm}^3 \text{g}^{-1}$
	N	N/C	N	N/C	pyridinic N <sup>[a]</sup>	pyrrolic N <sup>[b]</sup>	graphitic N <sup>[c]</sup>		
	wt.%	at./at.	at.%	at./at.	%	%	%		
MCs	-	-	-	-	-	-	-	847	2.6
NMCs	8.1	0.08	20.4	0.31	56.2	31.7	12.1	731	2.6

[a] the relative concentration of pyridinic N ( $398.5 \pm 0.3$  eV); [b] the relative concentration of pyrrolic N ( $400.5 \pm 0.3$  eV); [c] the relative concentration of graphitic N ( $401.6 \pm 0.3$  eV); [d] BET specific surface area; [e] total pore volume ( $P/P_0 = 0.985$ ).

In our synthesis approach, the incorporation of high-nitrogen-content melamine into phenolic precursors can transfer nitrogen atoms into carbon framework under pyrolysis conditions. The N/C mole ratio of NMCs is 0.31 determined from high-resolution XPS, three times higher than the value obtained from elemental analysis. The variation of the values can be explained by the surface specificity of XPS measurements, suggesting the N atoms are apt to gather in the surface rather than the bulk of carbon framework.

**Table S2.** Pore structure parameters of the MC/La<sub>2</sub>O<sub>3</sub> composites and NMC/La<sub>2</sub>O<sub>3</sub> composites

Sample	S <sub>BET</sub> <sup>[a]</sup> m <sup>2</sup> g <sup>-1</sup>	V <sub>T</sub> <sup>[b]</sup> cm <sup>3</sup> g <sup>-1</sup>
5La-MC	755	2.2
10La-MC	754	2.0
15La-MC	752	1.9
5La-NMC	674	2.4
10La-NMC	670	2.3
15La-NMC	668	2.1

[a] BET specific surface area; [b] total pore volume (P/P<sub>0</sub>= 0.985).

After incorporating La<sub>2</sub>O<sub>3</sub> onto the carbon framework, the porosity and the specific surface area show the expected decrease due to the introduction of heavier La<sub>2</sub>O<sub>3</sub> nanoparticles. Similar pore volume and S<sub>BET</sub> have achieved at the same La<sub>2</sub>O<sub>3</sub> loading, which help us avoid the complication of the different pore structures while focus on the nitrogen doping determined electrochemical performance afterwards.

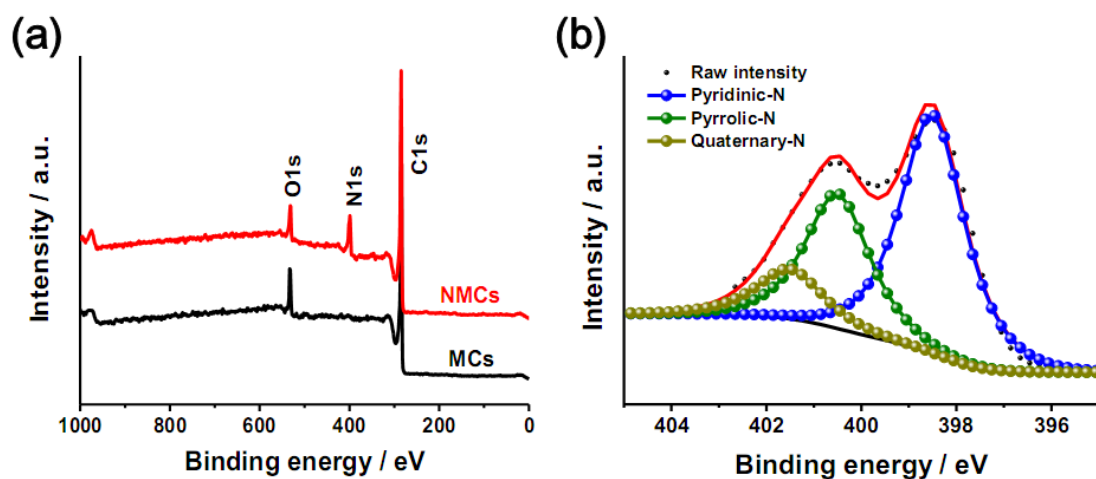


**Figure S1.** (a) XPS survey spectra of NMCs and MCs; (b) high-resolution XPS  $N_{1s}$  spectra of NMCs. A strong  $N_{1s}$  peak is observed for NMCs, while no obvious peak corresponding to nitrogen is found for MCs. The  $N_{1s}$  spectra were curve-fitted into three peaks with binding energies of 398.5, 400.5 and 401.6 eV corresponding to pyridinic N, pyrrolic N, and graphitic N, respectively.

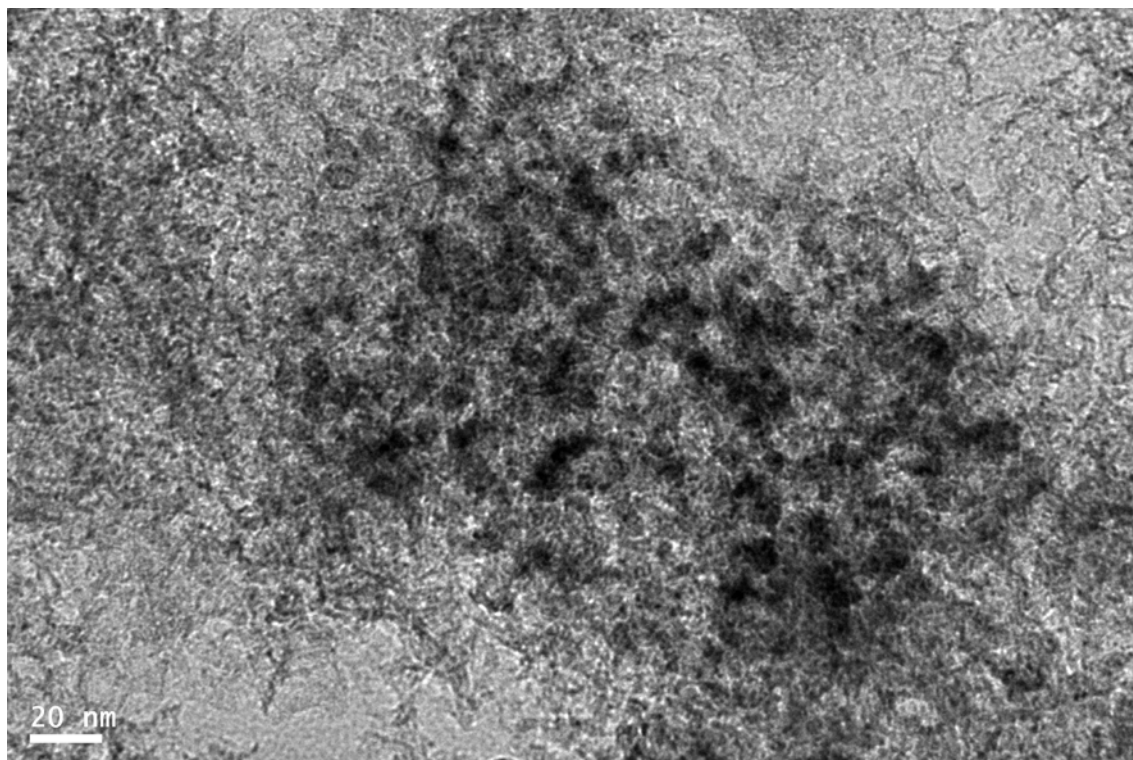


**Figure S2.** TEM image of 10La-MC composites. Some obvious  $\text{La}_2\text{O}_3$  aggregates could be observed in the nitrogen-free 10La-MC composites due to the Ostwald ripening and/or migration-coalescence of  $\text{La}_2\text{O}_3$  particles easily occur during the nucleation and thermal-decomposition process.

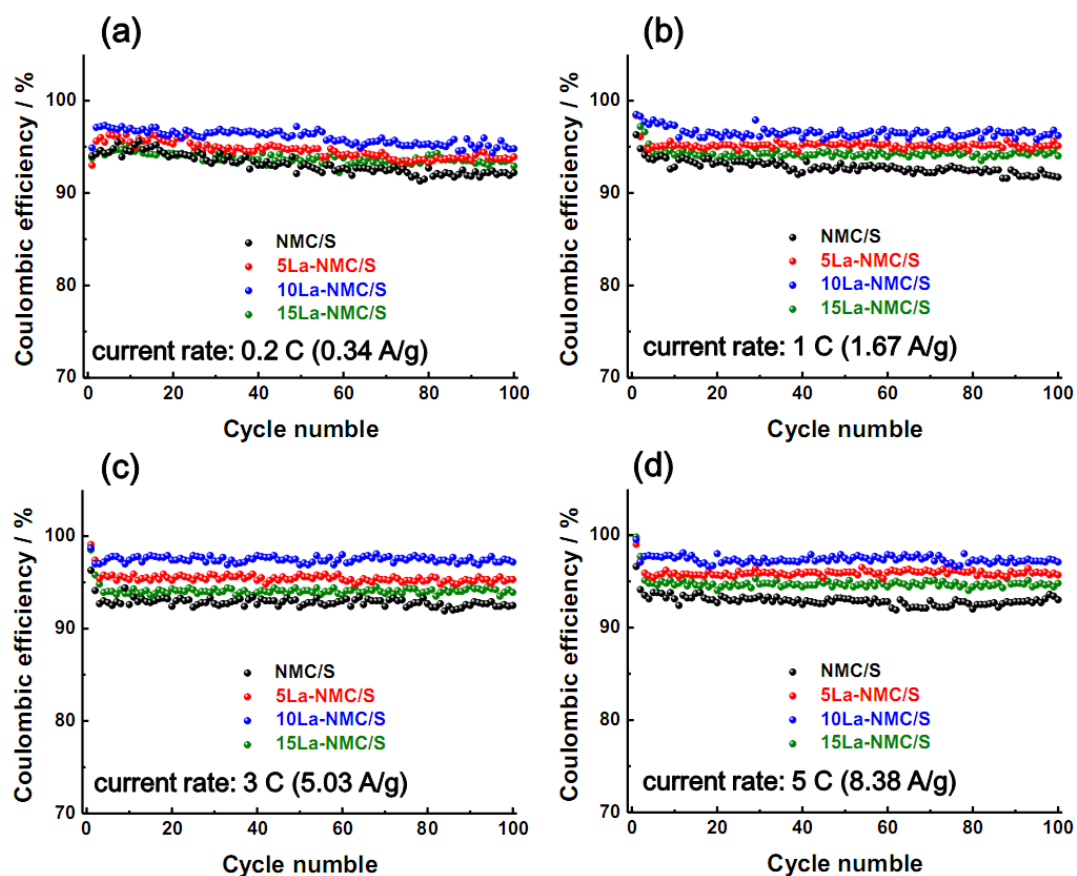


**Figure S3.** Coulombic efficiency of NMC/La<sub>2</sub>O<sub>3</sub>/S composites at 0.2 C (a), 1 C (b), 3 C (c) and 5 C (d).

With 10 wt.% La<sub>2</sub>O<sub>3</sub> decoration, the ternary 10La-MC/S composites exhibits coulombic efficiency of 94.9 %, 96.2 %, 97.1 % and 97.2 %, respectively at 0.2 C, 1 C, 3 C and 5 C after 100 cycles.

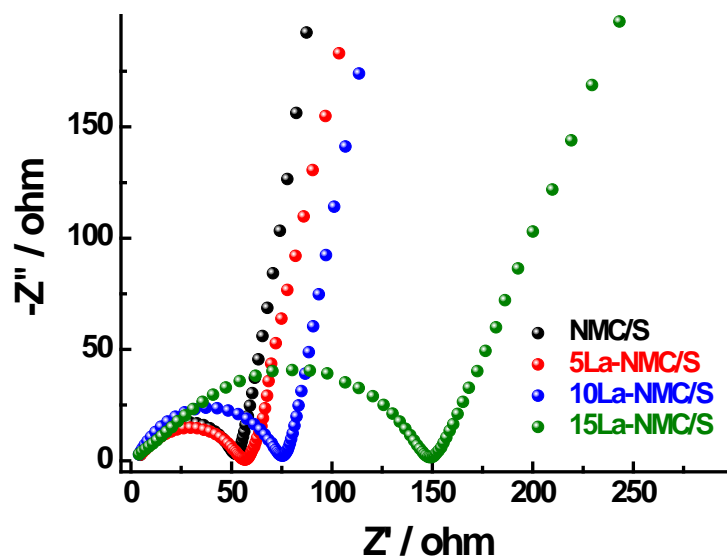


**Figure S4.** EIS before 1st cycle of NMC/La<sub>2</sub>O<sub>3</sub>/S composites. The semicircle diameters in the high frequency region of Nyquist plots indicate that the charge-transfer resistances are highest in 15La-NMC/S composites. The lowest electronic conductivity should be due to the excessive insulated La<sub>2</sub>O<sub>3</sub> decoration.

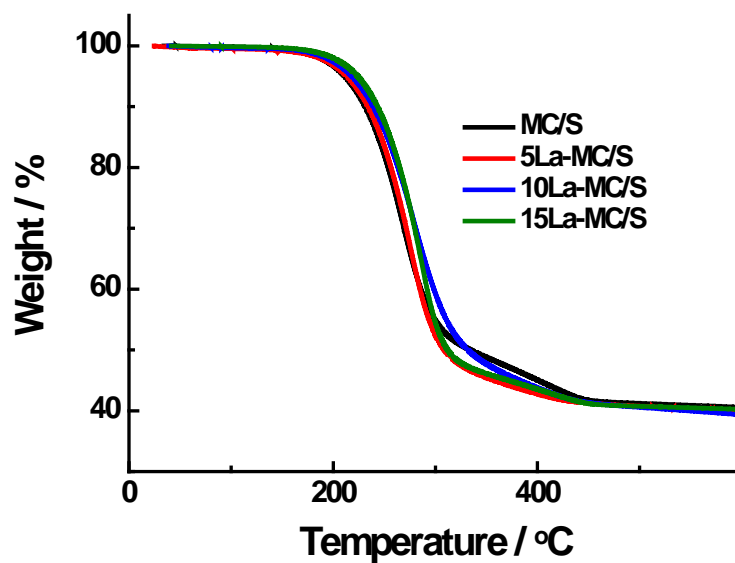


**Figure S5.** Thermogravimetric analysis (TGA) curves of MC/La<sub>2</sub>O<sub>3</sub>/S composites. The sulfur contents of the MC/La<sub>2</sub>O<sub>3</sub>/S composites are also carefully controlled at the same of 60 wt. % as that of the NMC/La<sub>2</sub>O<sub>3</sub>/S composites. This could thus minimize the influence of the sulfur content, which could prompt us to focus on the effect of the La<sub>2</sub>O<sub>3</sub> decorating and the nitrogen doping on the electrochemical performances of the resulting composites.

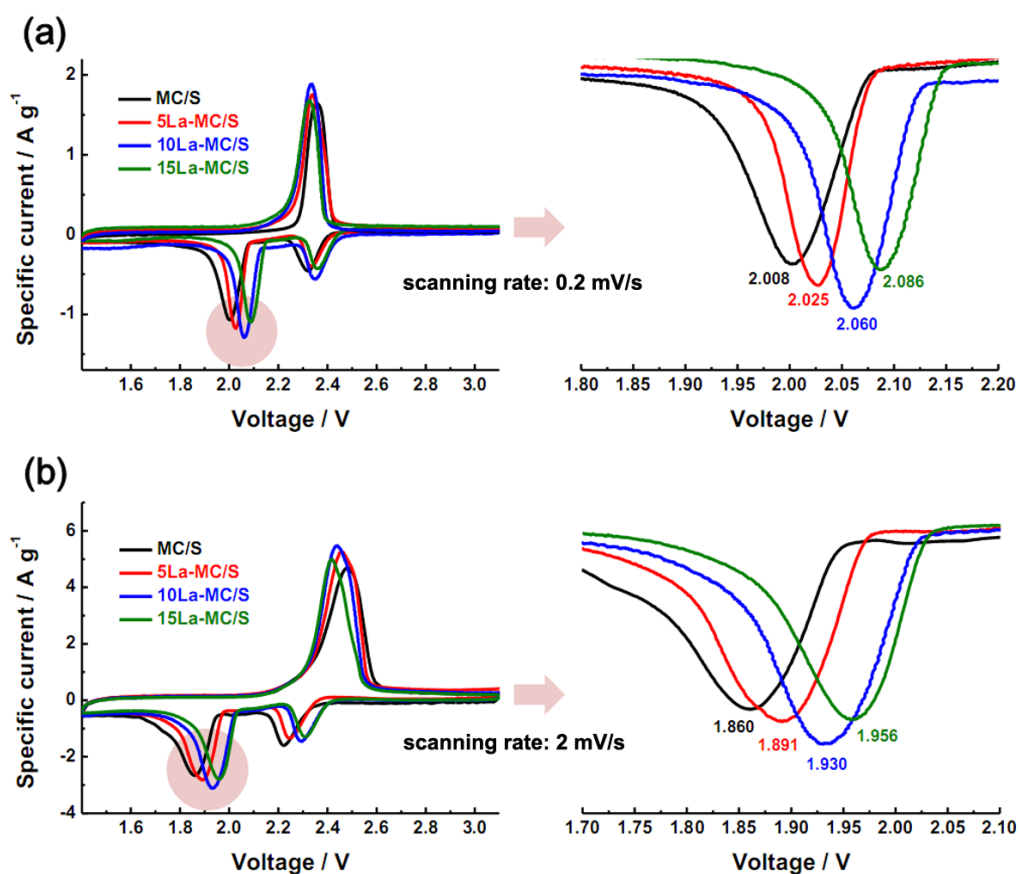


**Figure S6.** Typical cyclic voltammogram of nitrogen-free MC/La<sub>2</sub>O<sub>3</sub>/S composites at 0.2 mV s<sup>-1</sup> (a) and 2 mV s<sup>-1</sup> (b). Similar with the nitrogen doped NMC/La<sub>2</sub>O<sub>3</sub>/S composites, the sulfur reduction onset potentials gradually increase with the increase of La<sub>2</sub>O<sub>3</sub> loading, especially at a high scanning rate of 2 mV s<sup>-1</sup>. The higher reduction potential indicates improved kinetics by the La<sub>2</sub>O<sub>3</sub> decoration.

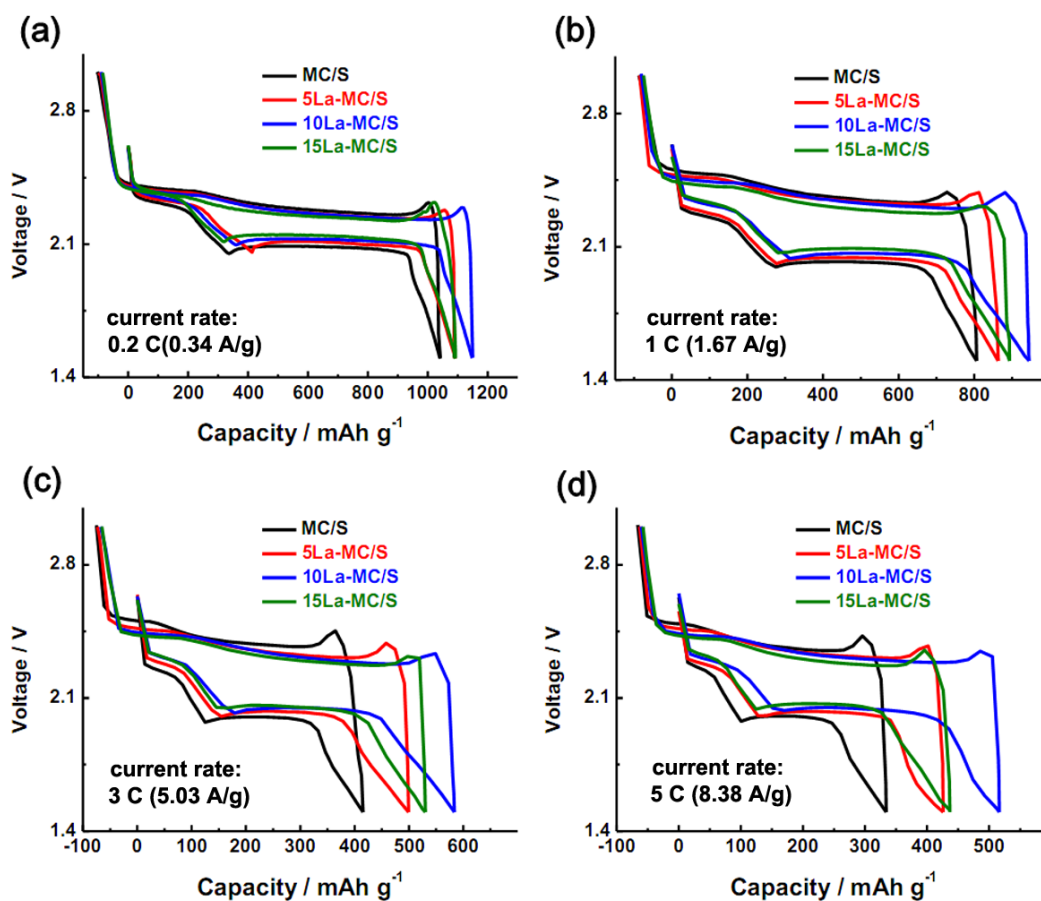


**Figure S7.** Initial charge-discharge curves of nitrogen-free MC/La<sub>2</sub>O<sub>3</sub>/S composites at 0.2 C (a), 1 C (b), 3 C (c) and 5 C (d). At a low rate of 0.2 C, the initial discharge capacity could be increased from 1041 mAh g<sup>-1</sup> (based on the mass of sulfur) for MC/S to 1149 mAh g<sup>-1</sup> by La<sub>2</sub>O<sub>3</sub> decoration. At a high rate of 5C (8.4 A g<sup>-1</sup>), the high initial discharge capacity of 514 mAh g<sup>-1</sup> could be achieved for 10La-MC/S, much improved compared to the capacity of 334 mAh g<sup>-1</sup> for MC/S.

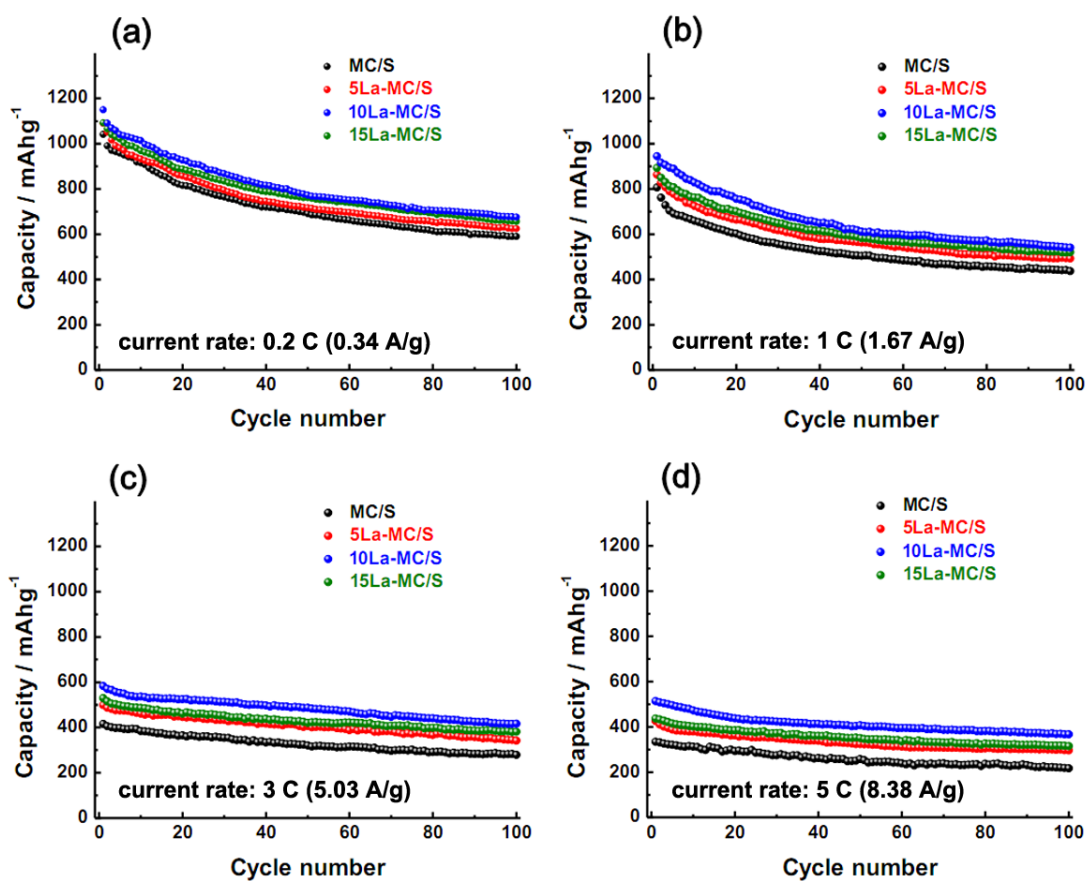


**Figure S8.** Cycle stability of nitrogen-free MC/La<sub>2</sub>O<sub>3</sub>/S composites at 0.2 C (a), 1 C (b), 3 C (c) and 5 C (d). With 10 wt.% La<sub>2</sub>O<sub>3</sub> decoration, the ternary 10La-MC/S composites deliver reversible capacities of 676, 541, 416 and 367 mAh g<sup>-1</sup> respectively at 0.2 C, 1 C, 3 C and 5 C after 100 cycles.

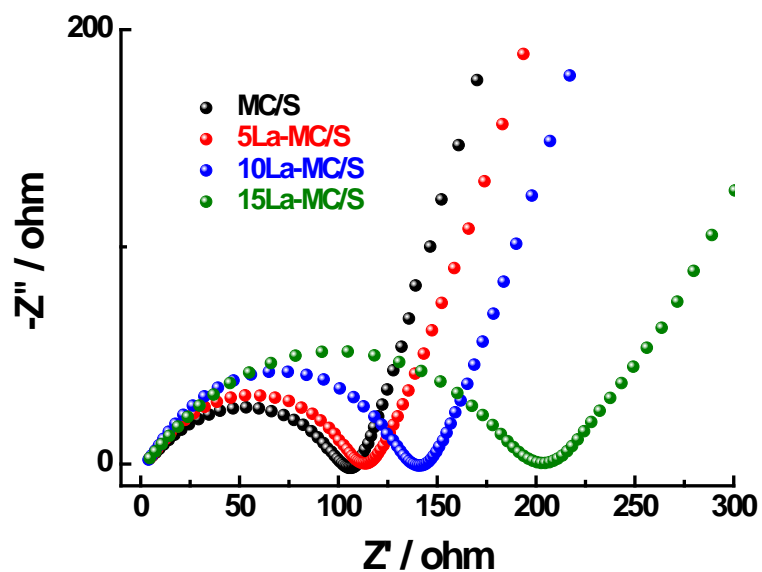


**Figure S9.** EIS before 1st cycle of nitrogen-free MC/La<sub>2</sub>O<sub>3</sub>/S composites. Similar with the nitrogen doped 15La-NMC/S composite, the 15La-MC/S composite also exhibits the highest charge-transfer resistances.